Opto-Electronic Advances

Supplementary information

2022, Vol. 5, No. 11

DOI: 10.29026/oea.2022.220058

Crosstalk-free achromatic full Stokes imaging polarimetry metasurface enabled by polarization-dependent phase optimization

Yaxin Zhang[1,3], Mingbo Pu[1,2,3]*, Jinjin Jin[1], Xinjian Lu[1,3], Yinghui Guo[1,2,3], Jixiang Cai[1,4], Fei Zhang[1,2], Yingli Ha[1,2], Qiong He[1], Mingfeng Xu[1,2], Xiong Li[1,3], Xiaoliang Ma[1,3] and Xiangang Luo[1,3]*

[1]State Key Laboratory of Optical Technologies on Nano-Fabrication and Micro-Engineering, Institute of Optics and Electronics, Chinese Academy of Sciences, Chengdu 610209, China; [2]Research Center on Vector Optical Fields, Institute of Optics and Electronics, Chinese Academy of Sciences, Chengdu 610209, China; [3]School of Optoelectronics, University of Chinese Academy of Sciences, Beijing 100049, China; [4]Key Laboratory of Optoelectronic Technology and System, Ministry of Education, Chongqing University, Chongqing 400030, China.
*Correspondence: MB Pu, E-mail: pmb@ioe.ac.cn; XG Luo, E-mail: lxg@ioe.ac.cn

This file includes:

Supplementary information for this paper is available at https://doi.org/10.29026/oea.2022.220058

Section 1: Numerical simulations

The responses of amplitude and phase spectra of the databases under linear and circular polarization lights illuminated from the substrate are simulated by CST. Moreover, the boundary conditions are unit-cell, unit-cell, and open along the *x*-, *y*-, and *z*-directions. Figure S1 depicts the responses of amplitude and polarization phase spectra in the entire scan space from 0.9 to 3.3 μm. The different *l* and *w* can provide various critical phase compensation for effective achromatic aberration.

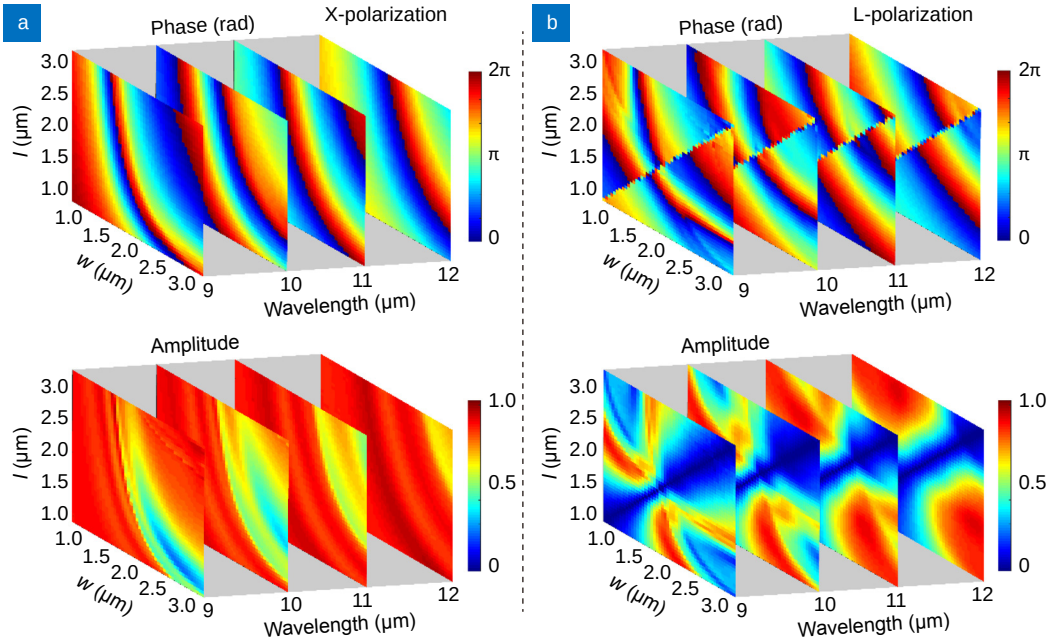

Fig. S1 | The database for broadband achromatic metalenses. (**a**) The amplitude and co-polarization phase spectra as a function of *l* and *w* under *X*-polarization incidence. (**b**) The amplitude and cross-polarization phase spectra for incident light with circular polarization.

Polarization detection is affected by the transmissivity of unit cells, depolarization effect, polarization response crosstalk, and other factors. On the one hand, we can normalize Stokes parameters as $S_1 = (I_X - I_Y)/(I_X + I_Y)$, $S_2 = (I_A - I_B)/(I_A + I_B)$, and $S_3 = (I_R - I_L)/(I_R + I_L)$, which method means that the transmissivity and depolarization of the metasurface are ignored in this analysis. On the other hand, the device needs to have crosstalk-free characteristic for accurate measurement. This feature indicates that the device has polarization selectivity and a high extinction ratio. We propose a polarization-dependent phase optimization method to reduce the crosstalk between orthogonal polarizations. The phase of the metalens satisfies Eq. (4) and Eq. (6) for linear and circular polarization, respectively. The particle swarm optimization (PSO) algorithm is adopted to meet the required phase, which can assist us in arranging the unit cells appropriately. The final optimization results are shown in Fig. S2. Figure S2(a) shows the phase matching of the X-polarization-sensitive achromatic metalens, where the response of the metalens to X-polarized light is shown in the upper. It can be seen that the optimized phase matches well with the ideal focused phase, proving that the designed achromatic metalens can focus X-polarized light. However, the response of the metalens to *Y*-polarization in the lower matches the diverging phase distribution, demonstrating that our device makes the orthogonal polarization state diverge, resulting in reduced crosstalk and improved extinction ratio. For circular polarization, we control the outgoing co-polarization to a divergent phase in the optimization. The phase match between desired phases and the co-polarization and cross-polarization parts of the metalens that regulates L-polarization are shown in Fig. S2(b).

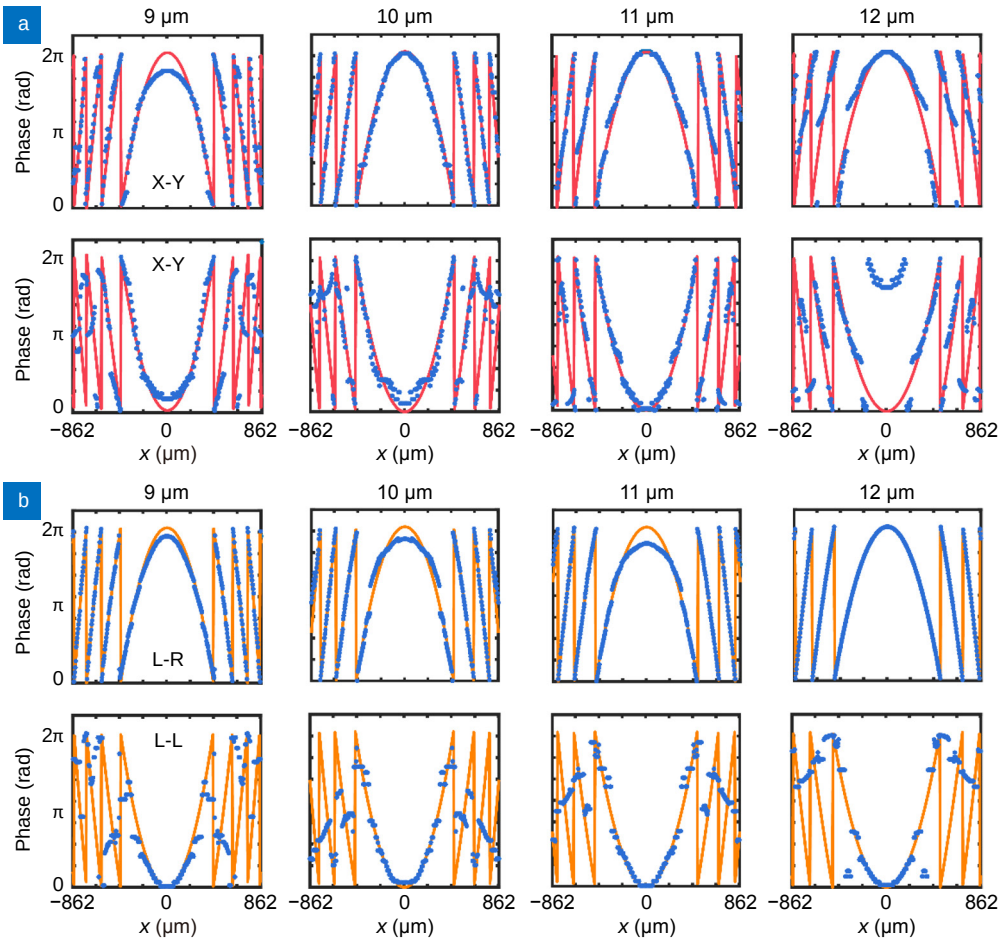

Fig. S2 | Comparison of optimized phase with ideal phase. (**a**) Phase response of X-polarization (top) and *Y*-polarization (bottom) for X-polarization-sensitive achromatic metalens (discrete dots) compared with the desired phase (solid line). (**b**) Cross-polarization (top) and co-polarization (bottom) responses of *L*-polarization-sensitive achromatic metalens (discrete dots) versus the desired phase (solid line).

To demonstrate the superiority of the optimized metalenses, we compare the present method with the traditional method, i.e., considering only the upper part of Eq. (4) and Eq. (6). We simulated the X- and Y-polarization-sensitive metalenses numerically under X-polarized incidence and L- and R-polarization-sensitive metalenses at L-polarized incidence, respectively. Fig. S3 exhibits the simulated focusing field intensity profiles of the metalenses in the *x*-*z* plane, the focal plane, and the cross-sectional $z = 0$ under L-polarized incidence with the wavelengths of 9, 9.3, 9.6, 10.3, 10.6, and 12 μm. The extinction ratios of the metalens designed based on our proposed method at the sampled wavelengths are 123.153, 70.843, 50.791, 84.001, 88.439, and 44.913, respectively. The extinction ratios of the metalens optimized by the conventional method at the sampled wavelengths are 17.591, 17.379, 24.945, 43.299, 35.799, and 38.548, respectively. The simulation results show that the extinction ratio of our design method is 7.001, 4.076, 2.036, 1.940, 2.470, and 1.165 times higher than that of the conventional method. The average extinction ratio increased over three times, which guarantees the measurement of the polarization state more precisely.

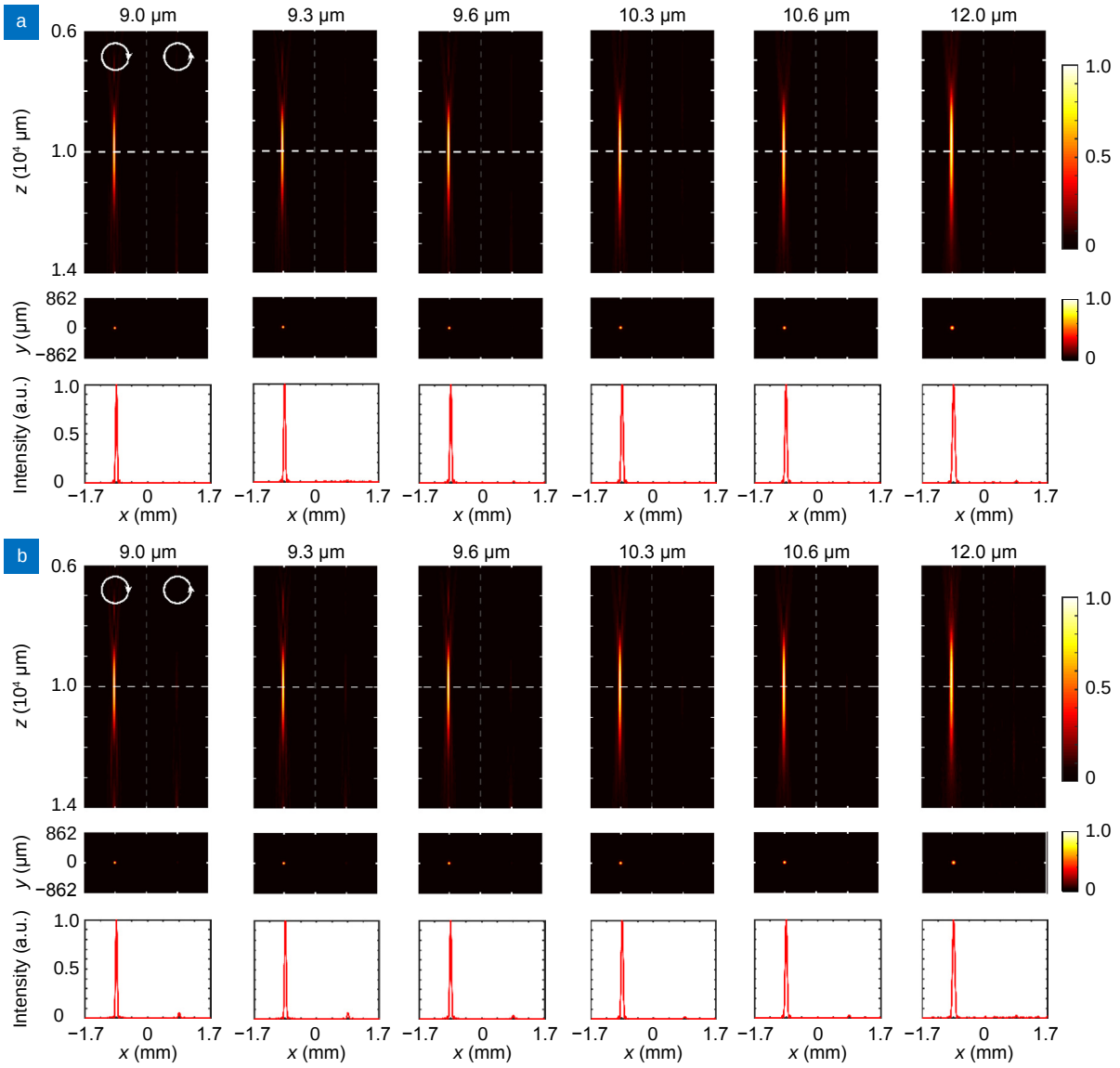

Fig. S3 | Simulation results of L- and R-polarization-sensitive metalenses designed with (**a**) polarization-dependent optimization method versus (**b**) conventional design method for L-polarized incident light. The upper diagram shows the intensity distribution in the *x*-*z* plane, and the white dashed line is the position of the focal plane. The middle figure is the focal plane intensity profile. The lower part is the normalized intensity profile along the white line.

Figure S4 shows the performance of the L and R polarization-sensitive achromatic metalenses. The designed metalens achieves achromatic focusing for L-polarized light, while there is no convergence effect for orthogonally polarized light, which is consistent with the expected result. The phenomenon of crosstalk-free between orthogonal circular polarizations ensures accurate measurement of circular polarization.

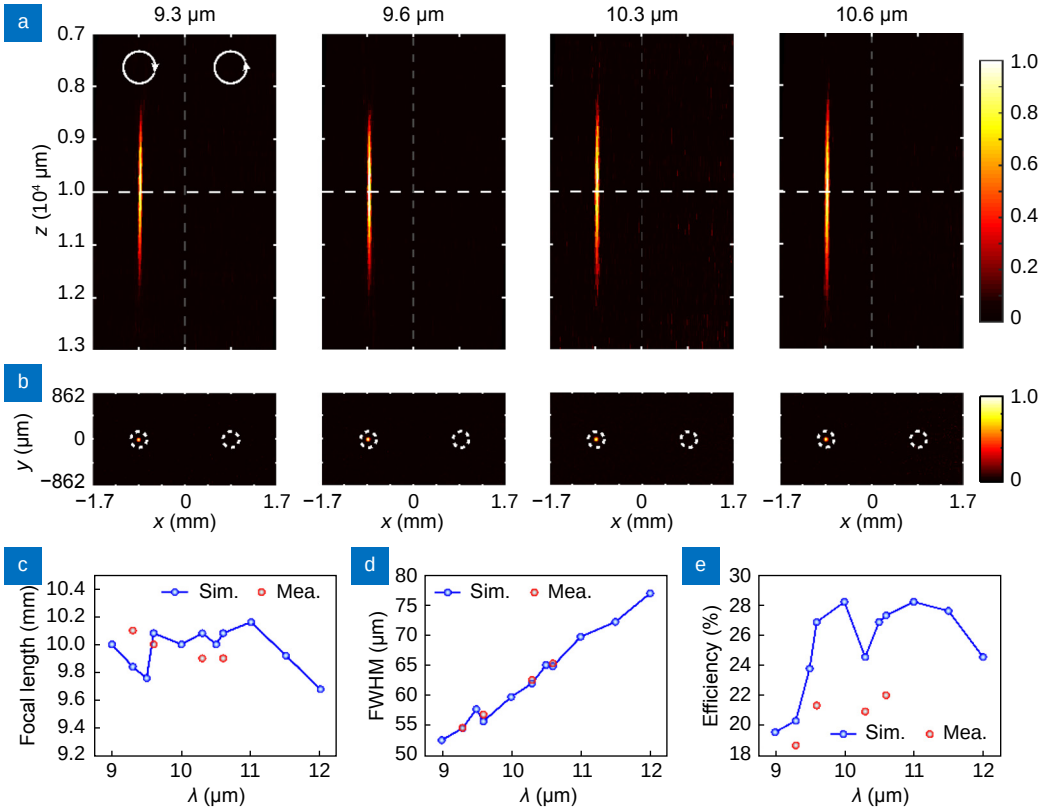

Fig. S4 | Optical performance of the broadband achromatic metalenses for circular polarization. (**a**) The measured intensity distributions of L and R polarizations sensitive metalenses in the *x*-*z* plane at various incident wavelengths for 9.3, 9.6, 10.3, and 10.6 μm under L polarized incidence. The white dashed lines are the position of the focal plane. (**b**) The measured focal plane intensity distributions. The extracted (**c**) focal lengths, (**d**) FWHMs, and (**e**) focusing efficiencies of the simulation and experiment are a function of wavelength. The blue solids represent the corresponding theoretical results at 9, 9.3, 9.5, 9.6, 10, 10.3, 10.5, 10.6, 11, 11.5, and 12 μm, and the red solids represent the experimental results at 9.3, 9.6, 10.3, and 10.6 μm. The experimental results are in good agreement with the theoretical results. Exp.: experiment. Sim.: simulation.

Section 2: Experimental setup and measured results

The optical setup for the designed polarimetry is exhibited in Fig. 5(c). A CO_2 laser (ACCESS LASER COMPANY L4GT), line polarizers (LP), and a quarter-wave plate (QWP) are used to generate arbitrarily polarized incident beams. In the characterization of the achromatic metalenses, the intensity profiles in the *x*-*z* plane and focal plane are measured by the infrared camera (GUIDE INFRARED Plug-612) placed on the electronically controlled translation stage (GCD-203050M, Daheng optics) to produce stable and uniform displacement, which is controlled by electric stage controller (GCD-040101M, Daheng optics) and controller power supply (GCD-040202M, Daheng optics). We measured intensity distributions at the focal plane and calculated Stokes parameters for different incident polarizations with various incidences when analyzing the polarization detection capability. The specific Stokes parameters measured in Fig. 6 are shown in Table S1–S4.

During the image process, we fabricate a polarization mask that consists of left and right-distribution metagratings, as shown in Fig. S5(a). In order to generate circularly polarized light, the metagratings are designed as quarter-wave plates with grating constant d = 2.3 μm, height h_1 = 2.9 μm, and slit width a = 0.7 μm. Left and right-side gratings are perpendicular to each other with the same parameters. The phase difference between the two orthogonal light waves along the short and long axes is around 90°, as shown in Fig. S5(b). When the polarization direction of perpendicularly incident light is 45° with the optical axis of the waveplate, the transmittance of different outgoing polarization light is shown in Fig. S5(c). Designed waveplates can produce circularly polarized light with high transmittance. The fabrication method of the mask is the same as the polarimeter, and its SEM image is shown in Fig. S5(d). In the experiment, a ceramic heating lamp combined with two filters (longwave-pass filter LP-9000 nm, Spectrogon and IR Bandpass Filter 11-999 (8–12 μm), Edmund) generates a 9–12 μm broadband light source. The polarization mask converts 45° polarized incidence into a preset pattern with polarization information characterized by the design imaging polarimeter, and the experimental setup is shown in Fig. S5(e).

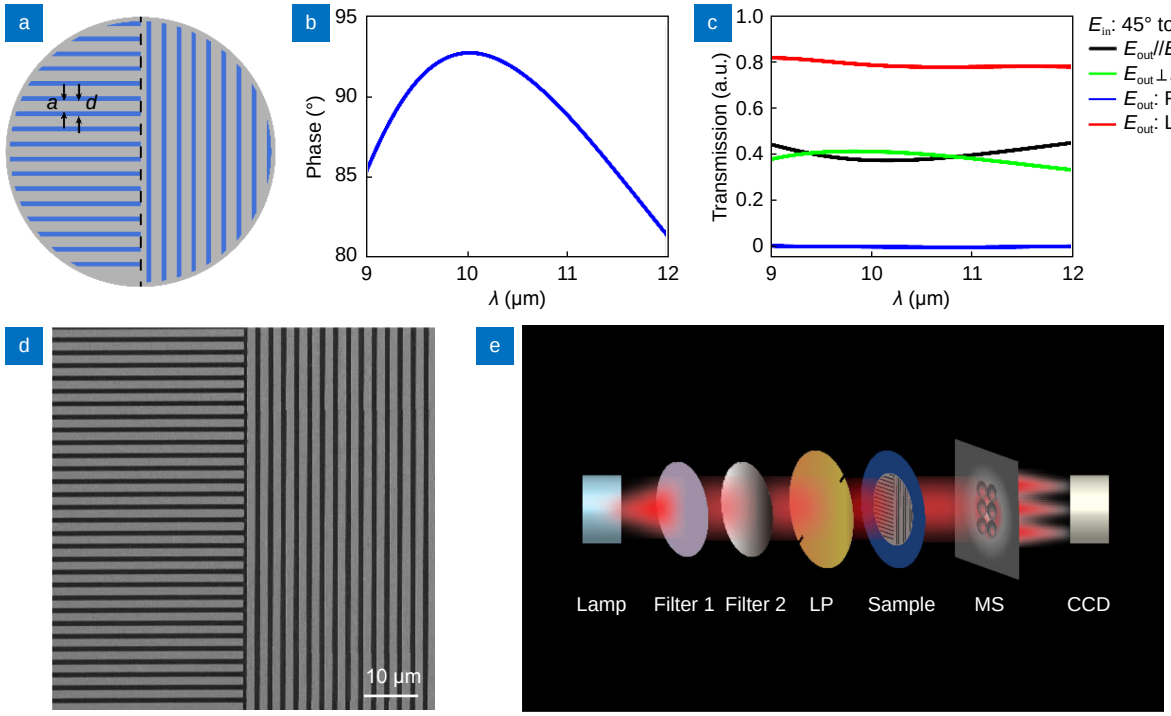

Fig. S5 | The polarization mask. (**a**) Schematic diagram of the polarization mask. (**b**) The phase difference between the two orthogonal light waves along the short and long axes. (**c**) The transmittance under different outgoing conditions when the polarization direction of the perpendicular incident light is 45° to the optical axis. (**d**) SEM image of the polarization mask. (**e**) The optical setup for imaging polarimetry. Optical elements: linear polarizer (LP), metasurface (MS).

Table S1 | Stokes parameters are measured at 9.3 μm.

Polarization	Theoretical(S_1, S_2, S_3)	Measured (S'_1, S'_2,S'_3)	Relative error
X	[1, 0, 0]	[0.932, 0.026, 0.009]	7.34%
Y	[–1, 0, 0]	[–0.926, 0.009, –0.081]	11.01%
A	[0, 1, 0]	[0.025, 0.931, 0.056]	9.23%
B	[0, –1, 0]	[–0.03, –0.946, –0.007]	6.26%
L	[0, 0, –1]	[0.023, –0.014, –0.961]	4.74%
R	[0, 0, 1]	[–0.04, –0.015, 0.919]	9.13%
30° linear polarization	[0.5, 0.866, 0]	[0.511, –0.858, 0.005]	1.48%
Elliptical polarization	[0.5, 0, 0.866]	[0.476, –0.070, 0.866]	7.44%
Average relative error			7.08%

Table S2 | Stokes parameters are measured at 9.6 μm.

Polarization	Theoretical(S_1, S_2, S_3)	Measured (S'_1, S'_2,S'_3)	Relative error
X	[1, 0, 0]	[0.930, –0.029, 0.047]	8.97%
Y	[–1, 0, 0]	[–0.961, 0.043, –0.043]	7.19%
A	[0, 1, 0]	[–0.063, 0.950, –0.080]	10.92%
B	[0, –1, 0]	[–0.056, –0.998, –0.017]	5.87%
L	[0, 0, –1]	[–0.057, –0.014, –0.924]	9.6%
R	[0, 0, 1]	[–0.04, –0.021, 0.909]	9.37%
30° linear polarization	[0.5, 0.866, 0]	[0.555, –0.838, –0.063]	8.78%
elliptical polarization	[0.5, 0, 0.866]	[0.515, –0.054, 0.805]	8.27%
Average relative error			8.62%

Table S3 | Stokes parameters are measured at 10.3 μm.

Polarization	Theoretical(S_1, S_2, S_3)	Measured (S'_1, S'_2,S'_3)	Relative error (%)
X	[1, 0, 0]	[0.959, –0.02, 0.047]	3.92
Y	[–1, 0, 0]	[–0.944, –0.092, 0.023]	10.56
A	[0, 1, 0]	[0.021, 0.946, 0.082]	10.04
B	[0, –1, 0]	[0.0037, –0.967, 0.003]	3.32
L	[0, 0, –1]	[0.058, –0.03, –0.953]	10.3
R	[0, 0, 1]	[–0.055, 0.036, 0.964]	8.91
30° linear polarization	[0.5, 0.866, 0]	[0.490, –0.831, –0.010]	3.80
elliptical polarization	[0.5, 0, 0.866]	[0.481, –0.032, 0.815]	6.34
Average relative error			7.15

Table S4 | Stokes parameters are measured at 10.6 μm.

Polarization	Theoretical(S_1, S_2, S_3)	Measured (S'_1, S'_2,S'_3)	Relative error (%)
X	[1, 0, 0]	[0.897, –0.074, 0.017]	12.81
Y	[–1, 0, 0]	[–0.947, –0.03, 0.008]	6.21
A	[0, 1, 0]	[–0.045, 0.929, 0.023]	8.70
B	[0, –1, 0]	[–0.013, –0.967, –0.105]	11.15
L	[0, 0, –1]	[0.058, –0.03, –0.953]	8.09
R	[0, 0, 1]	[–0.055, –0.036, 0.964]	7.52
30° linear polarization	[0.5, 0.866, 0]	[0.491, –0.832, –0.031]	4.72
elliptical polarization	[0.5, 0, 0.866]	[0.514, 0.003, 0.866]	1.46
Average relative error			7.59